Russian Chemical Reviews **64**(8) 767–781 (1995)
©1995 Russian Academy of Sciences and Turpion Ltd

UDC 541.138

Scanning tunnelling and atomic force microscopy in the electrochemistry of surfaces

A I Danilov

Contents

I.	Introduction	767
II.	Theoretical foundations of scanning probe microscopy	767
III.	Design of the tunnelling and atomic force microscopes	769
IV.	Applications of scanning probe microscopy in electrochemistry	773
V.	Prospects for the development of scanning probe microscopy	778

Abstract. The theoretical foundations, principle of operation, constructional features, and the latest advances in scanning tunnelling and atomic force microscopy in situ are examined in relation to electrochemical studies on the surfaces of metallic electrodes, and adsorption and electrocrystallisation processes. The bibliography includes 172 references.

I. Introduction

No one is surprised nowadays by communications concerning the observation of the morphology of surfaces at atomic resolution, although the scanning tunnelling microscope (STM) was invented by Binnig and Rohrer only just over 10 years ago.[1] At that time, it was difficult to believe that the observation of the atomic structure of a surface in vacuo or in air was realistic. Nowadays electrochemists are no longer satisfied with observations ex situ but prefer to use the STM or the atomic force microscope (AFM) for the investigation of the state of the electrode surface in situ during the polarisation process.

The term scanning probe microscopy (SPM), which combines tunnelling and atomic force microscopies because these methods have much in common and are frequently used simultaneously, has been established in the English language literature. Scanning probe microscopy is developing rapidly at the present time, an enormous number of publications concerning its use in electrochemical experiments have appeared, and the degree of sophistication of the research has greatly increased—from the demonstration of the possibilities of the instrument, investigators have gone on to a serious analysis of the results and a realistic study of the electrode surface and the mechanisms of the processes occurring on it. These factors have stimulated the writing of the present review. The principles of SPM and the traditional designs of the instruments are examined very briefly, as there are already many excellent review articles and monographs on this topic in the literature,[1–11] and attention is concentrated on the latest results of electrochemical studies and the prospects for the development of this unique method.

A I Danilov Laboratory for the Structure of Surface Layers, Institute of Physical Chemistry, Russian Academy of Sciences, Leninskii prosp. 31, 117915 Moscow, Russian Federation. Fax (7-095) 952 53 08. Tel. (7-095) 955 44 55

Received 14 March 1995
Uspekhi Khimii **64**(8) 818–833 (1995); translated by A K Grzybowski

II. Theoretical foundations of scanning probe microscopy

1. Principle of the operation of the tunnelling and atomic force microscopes

A real possibility of the tunnelling of an electron through a barrier, the height of which greatly exceeds its energy, is known to exist. If two conductors (electrodes), separated by a dielectric (vacuum, gas, or liquid), are brought together to a sufficiently short distance s and a potential U_t is established between them, then a tunnelling current I_t arises in the circuit, is proportional to the applied potential, and depends exponentially on the distance between the electrodes:

$$I_t = KU_t \exp(-A\sqrt{V_t}s), \quad (1)$$

where K is a constant, V_t the height of the potential barrier (for $s > 2$ nm, the height of the barrier is virtually equal to the electron work function), and $A \approx 10$ nm^{-1} eV$^{-1/2}$ is the proportionality coefficient. This is the Fowler–Nordheim equation, which is valid for planar electrodes and low potentials ($U_t \ll 1$ V). In real experiments such conditions are not always observed, but the exponential dependence of the tunnelling current on distance is retained (see, for example, Behm et al.[2] and Christensen[8]).

Simple calculation shows that, in order to record a tunnelling current of the order of magnitude of a nanoampere, it is necessary to bring the probe electrode to a distance of several angstroms from the surface investigated (for metals, $V_t \approx 5$ eV, and a tunnelling current of 1 nA is observed for $s \approx 0.6$ nm when $U_t \approx 1$ eV).[7]

Theoretically everything is fairly simple and it only remains to solve the problem of how the system is to be constructed.

The concept of the STM was proposed by Binnig and Rohrer in 1979, and in 1981 the first clear cut dependence of the tunnelling current on the distance between the specimen and the point of the probe, characteristic of tunnelling, was recorded. Topographical images of the $GaIrSn_4$ surface with multiatomic steps were soon obtained.[1]

The simplest tunnelling microscope (Fig. 1) consists of a piezoceramic scanner *1* (a tripod or sectioned tube, the geometrical dimensions of which vary in the XYZ directions following the application of an electric potential to the corresponding section) with a tunnelling probe *2* (a sharp needle made from tungsten, a platinum–iridium alloy, carbon, or another material), electronic circuits *4* for the maintenance of the potential and the tunnelling current in the test specimen *3* and the probe, and a recording and controlling computer system *5*.

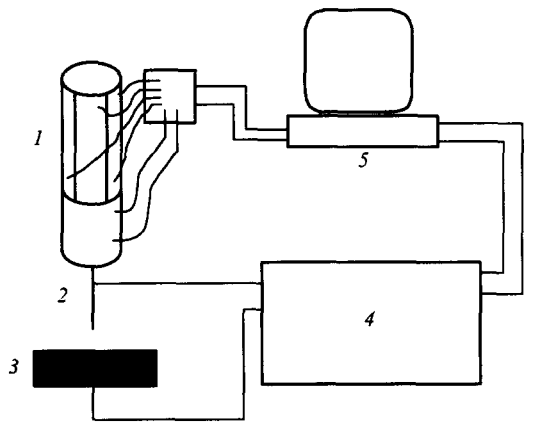


Figure 1. Block diagram of the tunnelling microscope (here and henceforth the explanations are given in the text).

Different designs of piezoscanners make it possible to move the point of the probe to distances ranging from fractions of an angstrom to several tens of micrometers. After the probe has approached the surface to a distance of several angstroms (the moving devices for the solution of this problem will be examined below), the tunnelling current assumes values of the order of magnitude of a nanoampere, and the electronic circuit with a feedback loop makes it possible to stabilise the current by varying the potential on the Z-section of the piezoscanner, i.e. by raising and lowering the probe (Fig. 2*a*) over the surface of the specimen (we recall that the tunnelling current depends greatly on the gap between the electrodes). The galvanostat works similarly, but here the potential on the electrochemical cell is varied in order to maintain a constant current in the working electrode circuit.

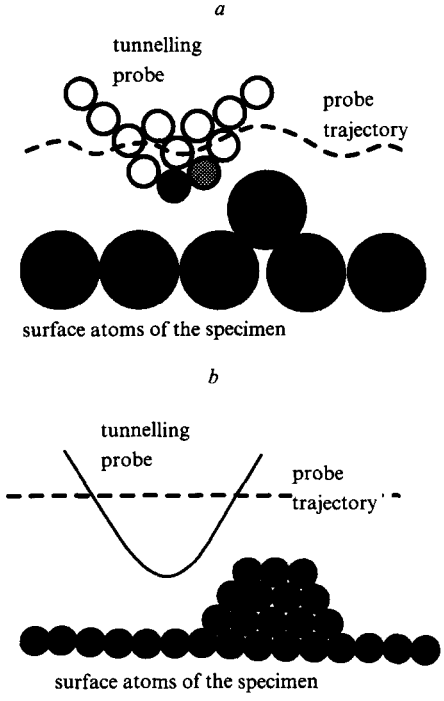


Figure 2. Principal regimes in the operation of the STM: (*a*) maintenance of a constant tunnelling current; (*b*) maintenance of a constant height of the probe over the specimen.

By applying to the X-section of the piezoscanner a potential varying linearly with time, it is possible to move the probe over the surface along a straight line (a ceramic unit, the length of which depends linearly on the applied potential, is used for piezoscanners). By recording the potential on the Z-section of the piezotube which is varied by the feedback loop, one obtains the surface relief along the scanning line. Strictly speaking, the electronic state of the surface and not its relief is recorded, but in most cases these relations are similar on specimens with a homogeneous composition. Thus, by varying the potential on the XY-sections and by measuring the displacements of the probe in the vertical direction, it is possible to scan a section of the surface and to obtain its topographic image. The correct employment of such images requires a careful calibration of the piezoscanners on objects with a known topography.

If the potential on the Z-section of the tube is fixed and the tunnelling current is measured with the probe moving above the specimen, it is possible to record the image of the surface more rapidly (Fig. 2*b*), but there is then an increase in the probability of 'sticking' because the feedback loop does not in this case control the current. This regime is suitable for the investigation of atomically smooth sections of the specimen and makes it possible not only to increase the scanning rate but also to improve the quality of the image by reducing the level of interference.

The sharpness of the probe is important—ideally there should be one atom at its end. Initially investigators wasted much time and effort on the preparation of very sharp needles by electrochemical or gas-phase etching. However, the exponential dependence of the tunnelling current on distance eliminated many problems—nowadays the majority of commercial STM employ mechanically sharpened probes or simply probes sliced at an angle. Under these conditions, some of the surface atoms of the probe are closer to the test surface than others and play the role of the sharp point. Naturally, it is best to have a sharp etched needle, since otherwise in recording the image of a rough surface one may obtain artefacts as a result of the alternate operation of several sections of a blunt needle which are at different times closer to surface projections. For example, in the situation illustrated schematically in Fig. 2*a* a lateral atom, closer to the projection, 'operates' instead of the lowest atom of the probe.

The next step in the development of SPM was the creation of the atomic force microscope.[12] The exponential dependence of the tunnelling current on the distance between the electrodes is of decisive importance for the attainment of the atomic resolution in the STM, whereas in the AFM a similar importance attaches to the pronounced dependence of the force F of the interaction between bodies on the distance between them R,

$$F(R) = \frac{C_1}{R^{13}} - \frac{C_2}{R^7}, \qquad (2)$$

where C_1 and C_2 are constants. The first term in the equation for the Lennard-Jones potential describes the short-range repulsion forces between the electron clouds of the atoms brought into contact, while the second term describes the attraction forces acting over relatively large distances. One of the bodies involved is the probe (the needle *1* fixed on a flat spring *2*), while the other is the test surface *3* (Fig. 3).

The problem of bringing the probe to the required distance from the steps of the specimen and scanning over the latter is solved, as in tunnelling microscopy, with the aid of the piezoceramic XYZ-translator *6*, while the vertical movements of the needle are recorded either with the aid of an optical system [in this case a laser beam is reflected from the mirror *4*, fixed on the spring *2*, and falls on the photodiode *5* (Fig. 3*a*)] or with the aid of the tunnelling probe *7* mounted over the spring *2* (Fig. 3*b*). The second variant requires a more complex control system and is used fairly rarely.

The AFM can operate in two main regimes.

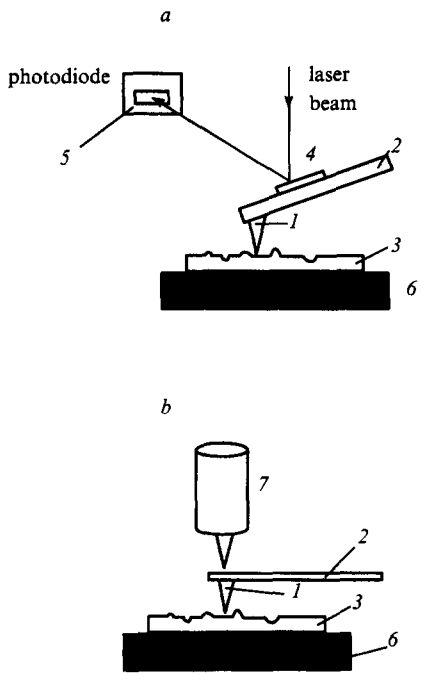


Figure 3. Principle of the operation of the atomic force microscope.

1. Contact-free interaction — the forces of attraction of the probe to the test surface are greater than the repulsion forces [see Eqn (2)]. With the aid of yet another piezocrystal, vibrations are induced in the needle at a frequency ν, which is close to the resonance frequency of the spring ν_r, and with an amplitude of about 2 nm (evidently the distance R between the needle and the specimen must be greater). In this case, the attraction force is determined[8] from the equation

$$\frac{dF(R)}{dR} = \frac{2k\Delta\nu}{\nu_r}, \qquad (3)$$

where $\Delta\nu = \nu - \nu_r$ is the change in the vibration frequency induced by the attraction of the probe to the surface and k is the elastic constant of the spring. The quantity $\Delta\nu$ is determined from the change in the vibration amplitude during the scanning by the needle over the surface of the specimen and the image is formed as the dependence of the force on the XY coordinate of the probe on the plane. Owing to the high vibration amplitudes, the needles must be kept at a considerable distance between the probe and the surface, which lowers the lateral resolution.

2. Contact interaction — repulsion forces predominate over short distances. In the simplest case, the probe acts as a gramophone needle and its vibrations in the vertical direction reflect the surface relief. In another variant of this method, the needle and the spring vibrate at a frequency of several hundreds of Hz with an amplitude of 0.5–2 nm (the needle is periodically in contact with the specimen and accurate values of the vibration parameters are selected for a specific rigidity of the spring). The decrease in the vibration amplitude of the needle as a result of the interaction of the probe with a rough surface is proportional to the height of the rugosities on the latter. During scanning along the XY coordinates, the specimen is moved upwards and downwards with the aid of a piezotranslator (in order to maintain a constant vibration amplitude) and the surface relief is thus recorded.

Atomic force and tunnelling microscopies are undergoing active development; compound devices in which an STM, an AFM, an electron microscope, and instruments for optical studies on surfaces are combined have been built.[13–17] Modifications of the AFM which make it possible to investigate the electrical and mechanical properties of the surface, have appeared,[14,16] but a detailed consideration of all these methods and designs is impossible within the framework of this review.

2. Tunnelling microscopy

As already stated, the tunnelling current is proportional to the potential between the electrodes U_t and depends exponentially on the height of the potential tunnelling barrier and on the distance between the probe and the test surface s. The propor-tionality coefficient K in Eqn (1) is determined mainly by the local density of the electronic states of the needle $[D_t(E_{F,t})]$ and the specimen $[D_s(E_{F,s})]$ at the Fermi level.[8] In the case of the clean uniform surfaces of metals, these quantities are independent and the use of Eqn (1) is fully justified. However, when an adsorbate or formations comprising foreign phases are present on the specimen, the density of the electronic states D_s can no longer be regarded as constant and the tunnelling current depends on the electron work function at the given point on the surface.

In the scanning of an electronically nonuniform surface of a specimen (for example, one with inclusions of foreign atoms) in the constant current regime, the variation of the height of the needle over the plane of the specimen no longer reflects the topography of the surface: a hump is observed over atoms with a low electron work function, whereas hollows are seen over atoms with an increased work function. Thus a problem of separation of the electronic and topographic effects arises in the analysis of the image.

This problem may be solved by means of scanning tunnelling spectroscopy (STS), the essential feature of which involves the measurement of the dependence of the tunnelling current I_t on the potential between the electrodes U_t for a fixed position of the probe above the surface.[2,6,8,18–21] In a modification of the regime involving a constant height of the probe (when a low variable potential is applied to the Z-section of the piezoscanner), it is possible to determine the function $I_t(s)$ for a constant value of U_t and fixed XY coordinates, but with the height of the probe over the surface of the specimen being varied within certain limits. In practice, one usually measures the differential signal dI_t/dU_t or dI_t/ds and then the electron work function at the given point on the surface is determined from the dependence of dI_t/dU_t on U_t (or of dI_t/ds on s). By carrying out such measurements at different points, one obtains a distribution map for the inclusions (the adsorbate, oxides, or other nonuniformities) on the surface of the specimen.

III. Design of the tunnelling and atomic force microscopes

We shall now consider the principal units of the tunnelling and atomic force microscopes. Since foreign commercial microscopes are as a rule not available to Russian investigators because of their high price and the lack of the necessary service arrangements, many investigators have attempted to construct such instruments independently and have achieved considerable success. The information presented here may therefore prove useful to those chemists who recognise the need for the employment of SPM in their research but have not yet gained sufficient experience for the independent construction of an instrument. Furthermore, the knowledge of the design of the apparatus enables beginners in the use of SPM to avoid artefacts in their investigations and in the treatment of the results.

1. The piezoscanner and tunnelling probe

The piezoscanner is the heart of the tunnelling and atomic force microscopes. This device actually makes it possible to move the probe to the required point over the test object and to carry out the measurements necessary to obtain information about the topography or electronic state of the surface.

A tripod (three linked, mutually perpendicular piezoceramic plates), on which a tungsten or platinum needle was mounted, was employed initially for this purpose. By varying the potential of the corresponding plates of the tripod, it is possible to move the probe along three coordinates and to analyse the surface. Recently, however, the tripod has virtually ceased to be used and has been replaced by the piezotube.[22] After special treatment of the piezoceramic (annealing and polarisation in an electric field in order to create the necessary orientation of the domains) and sectioning, such a tube (Fig. 4) makes it possible to scan a section of the surface and ensures the Z-translation of the probe over a range of several micrometers.

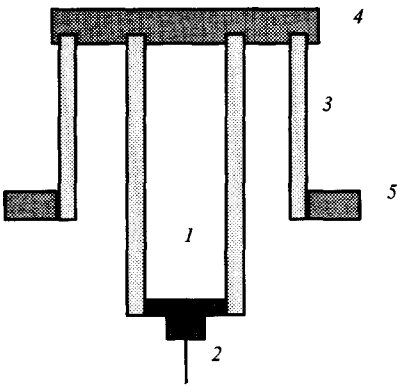


Figure 4. Schematic representation of the piezoscanner: (*1*) inner piezotube with a capacity for XYZ-movements; (*2*) tunnelling probe (needle with holder); (*3*) outer piezotube for the Z-movements and thermocompensation; (*4*) and (5) supports.

The tubular piezoscanner has many advantages over the tripod. It is more compact and more rigid, which means that it has a higher resonance frequency (in the development of the design of the STM, one must endeavour to achieve the highest possible resonance frequency of the scanner and the lowest possible resonance frequencies of the mechanical parts of the instrument in order to reduce the harmful effect of vibrations and acoustic interference). Furthermore, the use of two piezoceramic tubes of different diameter (Fig. 4) makes it possible to extend the scanning range and to reduce appreciably the effect of thermal drift on the measuring process as a consequence of thermocompensation along the Z coordinate.

The range of the movements of the scanner is determined by the nature, structure, and geometrical dimensions of the piezoceramic. For example, the thinner the walls of the tube, the greater the strength of the electric field which can be achieved within the ceramic and the larger the movements of the probe at the end of the tube which can be ensured in scanning the test surface.

The attachment of the probe to the scanner (screw, chuck, magnetic, and other needle holders are used) must ensure the necessary rigidity and at the same time make it easy to replace the needle under operating conditions. Furthermore, this unit must have the smallest possible weight because an increase in the mass of the scanner lowers its resonance frequency. The needle itself must also be fairly rigid and therefore must not be too thin and long.

Needles made of platinum–rhodium or platinum–iridium wire (iridium content 10%–30%) 0.2–1.0 mm in diameter have been most popular recently. In contrast to the tungsten needles, they are hardly oxidised in air at room temperature, are stable in corrosive media (acids and alkalis), and do not introduce impurities into the solution in the course of the experiment.

The platinum–iridium needles are sharpened by electrochemical etching in a 3 M NaCN + 1 M NaOH solution[23] or in a mixture of saturated $CaCl_2$ solution, concentrated HCl, and water in proportions of 60:4:36 by volume[24] at a constant or variable potential $U = 10 - 40$ V. A loop of platinum wire with an electrolyte film is usually employed as the counterelectrode in the cell (Fig. 5*a*).

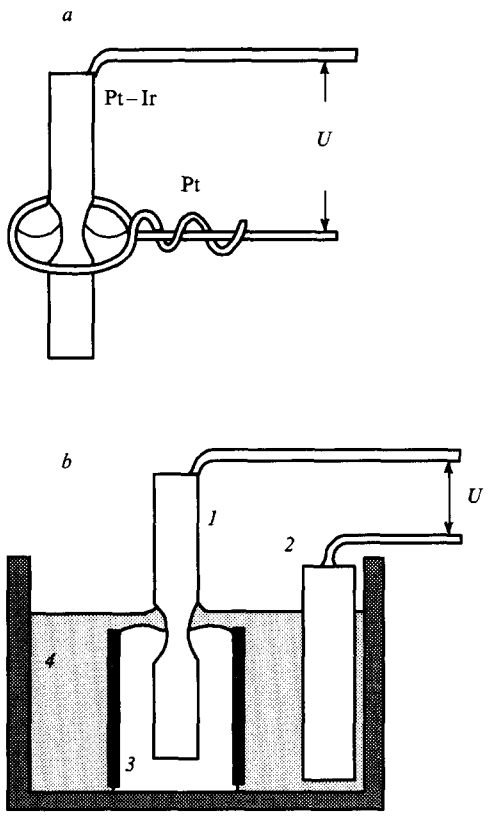


Figure 5. Electrochemical sharpening of the needles: (*a*) etching by means of a wire loop with an electrolyte film; (*b*) etching by immersion in a vessel with electrolyte.

The platinum–iridium alloy dissolves in the meniscus, while the part of the wire (about 1 cm long) below the film of solution serves as a weight which ensures the rupture of the wire when it becomes sufficiently thin. Tungsten needles are etched similarly in 2 M NaOH solution at a constant or variable potential of 1–15 V.[7,8]

The method described is not always convenient. When thick probes are employed, the etching time is several minutes and the electrolyte film can be disrupted as a result of the vigorous gas evolution. In such cases (Fig. 5*b*), the wire *1* from which the needle is to be prepared is lowered vertically into the vessel with the etch solution *4* and the auxiliary electrode *2* to a depth of about 1 cm. The immersed part of the wire is either insulated to prevent its dissolution or an air-filled glass capillary *3* is employed.[25] It is noteworthy that the upper part of the wire also has a sharp end if the current is interrupted immediately after the breaking away of the lower part.

Satisfactory results in the sharpening of platinum or platinum–iridium needles by treatment in a mixture of $CaCl_2$, water, and acetone followed by micropolishing in aqueous sulfuric acid solution have been obtained.[26] The authors were able to avoid the use of toxic cyanide solutions and to obtain smooth readily reproducible needles with a radius of curvature less than 10 nm.

Fairly numerous studies have been devoted to the technology of the preparation of sharp needles and these have been reviewed.[27]

In an experiment in solution, the Faraday current I_F due to the electrochemical reaction on the surface of the needle passes through the latter in addition to the tunnelling current. Reliable information about the topography of the working electrode can then be obtained only subject to the condition $I_F \ll I_t$. This is achieved in two ways: either the probe potential is maintained in the region corresponding to the minimum Faraday current or virtually the entire surface is insulated by a nonconducting material allowing only the minimum possible section on the very end of the needle to remain 'operational'. Glass or polymers are used as insulators; insulation with the aid of the thermoplastic material Apiezon wax is fairly popular.[3]

One of the main problems in the insulation of needles is to ensure that the area of the active surface of the probe does not exceed 1 μm^{-2}, which corresponds to $I_F < 0.1$ nA. It is sometimes simpler to cover the entire surface of the needle with the insulator and then 'expose' its end by means of heat treatment, the application of a powerful electric field, ionic etching, or in some other way.

A novel method for the insulation of needles has been proposed by Mao et al.[28] They use a polymer, deposited from solution by means of an electric current, as the insulating coating. In order to make sure that the insulator on the end of the needle is not too thick (otherwise the problem of the electrical and diffusional screening of the section of the working electrode underneath the probe arises in the course of the STM experiment), electrophoresis is carried out on the needle the end of which is immersed in a drop of mercury. The needle is slowly withdrawn from the drop and at the instant of rupture of the electrical contact between the needle and mercury the coating deposition current is automatically switched off.

The method for the preparation of insulated platinum–iridium needles proposed by Bach et al.[29,30] is the simplest and most convenient. A mechanically or electrochemically sharpened needle is immersed in a solution of polyacrylic acid partly neutralised by a base (Glassophor ZQ 84-3225, produced by the BASF Company, Germany) and electrophoresis is carried out with a platinum cathode at a potential of 25–70 V. The decomposition of water on the anode leads to the acidification of the near-electrode space, as a result of which the polymer passes to a sparingly soluble form and is deposited on the platinum–iridium needle as a film. Further polymerisation, designed to strengthen the coating, is achieved by means of heat treatment ($\sim$200 °C for several minutes), whereupon the chemical stability of the polymer increases and the very end of the needle is exposed as a result of thermocontraction.

With the aid of needles insulated in this way, it has been possible to determine the structures of atomic adsorbed layers of copper on gold.[30] This fact indicates the high quality of the probe and the absence of impurities from the test solution. Stationary Faraday currents of the probe in 0.2 M KCl + 0.01 M $K_3Fe(CN)_6$ solution do not exceed 0.2 nA, which corresponds to an area of the active surface of the needle equal to the area of a circle with a radius less than 0.1 μm.[30] The 0.2 M KCl + 0.01 M $K_3Fe(CN)_6$ solution is frequently used to characterise microelectrodes by means of cyclic voltammetry or stationary methods.[31]

2. The polarisation circuit

When STM is used to investigate the behaviour of electrochemical systems, studies in which the measurements are performed with monitoring of the potential of the working electrode are of greatest interest. In this case, the probe is the fourth electrode in the cell and its potential is specified (measured) relative to the working electrode or the reference electrode. The usual potentiostat and a three-electrode cell were used initially[32–34] for the polarisation of the working electrode, the probe potential being determined from the tunnelling potential between the specimen and the probe:

$$E_t = E_s + U_t, \tag{4}$$

where E_t and E_s are the potentials of the probe and the specimen respectively.

Recently, however, virtually all investigators have used a bipotentiostat, similar to that employed for the polarisation of a disc electrode with a ring.[35] It permits the independent monitoring of the potential of the specimen and the probe relative to the reference electrode (from which the tunnelling potential is equal to the difference between the above potentials).[36–40] The bipotentiostat differs from the usual potentiostat in that, to obtain an image in the STM, it is necessary to ensure the operation of the feedback loop which maintains a constant tunnelling current, i.e. the cell polarisation circuit and the circuit for the control of the Z-movement of the piezoscanner must be adjusted for mutual consistency.

There is one circuit, with optical decoupling, which makes it possible to record the image at high Faraday currents without insulating the needle.[41] A similar circuit has been used[42] to investigate the initial stages in the deposition of copper on pyrographite. After each scan along the X coordinate, the needle is raised, the feedback loop is switched off, and the Faraday current due to the electrochemical reduction of oxygen on the probe is measured (in the quoted instance, $I_F \approx 40$ nA, tunnelling current $I_t \approx 0$). The current I_F is subtracted from the overall current of the needle, lowered to place it in its working state, the appropriate potential being applied from a digital-analogue converter to a summator, and the feedback loop is switched on again to maintain a constant tunnelling current $I_t \approx 4$ nA. Thus, after each scan the Faraday current is corrected, which makes it possible to record the image of the surface. The usual potentiostat-galvanostats with a three-electrode signal are used for atomic force microscopy.

3. Design of the moving device

Piezoscanners usually have a range of Z-displacements of the order of magnitude of 1 μm, so that the maintenance of a constant tunnelling current requires that the probe be brought to a distance $s < 1$ μm from the test surface without sticking the needle into the specimen. This problem is solved in different ways in various designs of the STM.[3,43–48] We shall consider some of them.

a. Mechanical moving devices

The microscrews employed initially in optical apparatus were some of the first to be used. Differential screws combined with a reduction gear ensure fairly small translational displacements of the order of several micrometers of linear movement per turn of the screw. Here it is necessary to solve the problem of play and of the stability of the position of the moved piezoscanner after the attainment of the specified point. Repeated scanning for a long time is sometimes needed for the analysis of the surface in experiments employing the STM. The stability of the position of the piezoscanner is adversely influenced by thermal drift and the relaxation of the mechanical stresses arising as the moving system actually moves.

Computer-controlled step motors are usually employed to automate the moving device — they make it possible to rotate the shaft of the screw by hundredths of a turn with a high accuracy.

b. Piezoelectric moving systems

The range of variation of the geometrical dimensions of the piezo-ceramic tube does not usually exceed several micrometers and the moving device must ensure the movement of the scanner by a fraction of a millimetre. The gap between the specimen and the probe can be set more accurately by hand in the preparation of the experiment, but the probability of random touching increases under these conditions.

The question arises how to increase the range of movement. Imagine the movement of a caterpillar. It gets hold of a leaf with its rear legs, lifts its front legs, and stretches. It then fixes the front legs on the leaf, raises its rear legs, and draws them forward, contracting its body.

The piezotranslator can work similarly. It is only necessary to find a way of fixing a particular end between the expansion/contraction stages.

The piezoelectric 'creeping worm' motor (Inchworm, Burleigh Instruments, Inc.), which ensures the movement of the piezoscanner by several millimetres with a minimum step of 1 nm and a rate up to 0.5 mm s^{-1}, may serve as an example of the mechanical fixing in the majority of commercial STM.[3] Fig. 6 presents a simplified diagram of this motor. The lower part of the motor contains the piezoceramic tube *1*, attached by the holder *5*, with upper (*2*) and lower (*3*) piezofixing devices. The slider *4* with the piezoscanner (not shown in the diagram) is located within the tube.

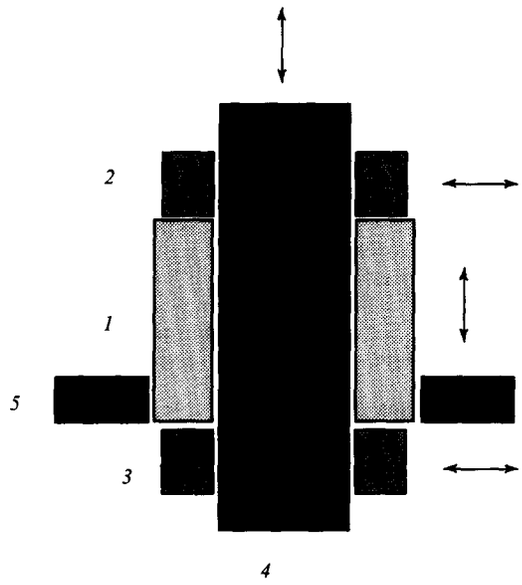


Figure 6. Design of the Inchworm piezoelectric motor. The arrows indicate the directions of the possible movements of the motor components.

In the static state, the fixing devices *2* and *3* grasp the slider from two sides by application of the appropriate pressure. In order to move the slider downwards, the fixing device *2* is released, the pressure on tube *1* is increased, and the latter becomes longer; the fixing device *2* is then applied again, while the fixing device *3* is released, whereupon the pressure on the tube is smoothly reduced. The tube contracts and pulls the slider with the piezoscanner. Thus the slider is alternately 'grasped' by the fixing devices and moves over a distance of up to 2 μm in one step. A very high precision in the treatment of the surfaces and the selection of the appropriate materials, which do not respond to changes in atmospheric humidity and exhibit a high resistance to wear and a low sliding friction, is necessary to ensure the stable operation of the motor.

A motor of simpler design may be made by employing magnetic or electromagnetic fixing devices, but here too it is necessary to overcome numerous difficulties to ensure smooth movement and the stability of the working position.

A somewhat different principle has been applied by Wildoer et al.[43] The slider is held in the resting position not by piezoelectric fixing devices but by flat springs adjusted in such a way that a slow increase in the length of the tube leads to a movement of the slider together with its free end by the frictional force, and a sharp contraction of the tube results in sliding. By applying a sawtooth potential to the piezotube, it is possible to move the slider over considerable distances.

The quality of the treatment and the selection of the materials are also very important in this design—the authors employed stainless steel coated with titanium carbonitride in order to diminish the coefficient of friction and to increase the resistance to wear of the slider and the flat springs.

4. Vibro- and sono-insulation

In order to obtain a high-quality image, it is necessary to achieve a low level of interference from electromagnetic, acoustic, and mechanical influences.[3,8] For this purpose, the measuring block of the STM is mounted on a fairly massive vibroinsulating platform. Spring or rubber suspensions, Viton ring washers,[49] or simply a half-deflated automobile inner tube provide effective protection against mechanical vibrations. In order to reduce the harmful effect of acoustic vibrations, use is made of metallic or glass jackets with sound-absorbing coatings. The earthed metallic jacket at the same time shields the measuring system from electromagnetic influences, but in this case visual monitoring of the state of the electrochemical cell is difficult.

The atomic force microscope is more stable towards low-frequency vibrations than the tunnelling microscope because the resonance frequencies of the springs usually exceed 10 kHz for the AFM whereas the typical vibrations of buildings have frequencies of the order of 20 Hz and an amplitude of about 1 μm. Since the amplitude of the induced vibration, A, is given by

$$A = A_0 \frac{v^2}{v_0^2}, \tag{5}$$

such vibrations at the resonance frequency induce vibrations with an amplitude of only 0.004 nm. This simple calculation[8] shows that, in contrast to the STM, the atomic force microscope hardly requires special vibroprotection in order to achieve atomic resolution.

5. Treatment of the image

When the test surface is scanned by the tunnelling probe, the primary image is usually produced in the form of a map of the distribution of the measured parameter (tunnelling current, height of the relief, etc.) on the scanning plane. Modern computers ensure a fairly high resolution and a wide colour range for a clear representation of the information obtained as a result of such scanning. There are numerous graphic programs which make it possible to edit the image and view the surface in two and three dimensions, but in work with the STM a special program is needed which combines at least the control of the movement of the probe towards the surface, the monitoring of the electrochemical behaviour of the system, the production of the image, and its primary processing.

We shall deal briefly with the processing of the images, concentrating attention on the risk of artefacts. The principal rule required to avoid such errors is that one should endeavour to obtain a high-quality image without resorting to methods for its improvement by means of computer programs. If all the precautions needed to reduce the level of interference have been taken and the image still remains subject to noise, it is necessary to understand the cause of such noise. It may be that it is a characteristic property of the system investigated and not an induced interference. For example, the presence of halides in the electrolyte is usually accompanied by an increase in the noise in the image because of the increase in the mobility of surface atoms.[50–52]

Digital filtration of images helps in many instances to increase the contrast in the image (or, conversely, to reduce it) for the subsequent analysis of the topography of the surface, but this method must be used with very great caution since, with the aid of Fourier transformations for example, it is possible to see a periodic structure in cases where it has never existed.

There are also computer program methods for the elimination of image defects[5,53] associated with the drift of the system and the nonparallel arrangement of the scanning and specimen planes,[54,55] the nonlinearity of the movement of the tunnelling probe in the scanning of the surface,[56] etc.

IV. Applications of scanning probe microscopy in electrochemistry

Scanning probe microscopy has provided unique possibilities for the investigation of the atomic structure of the electrode and has made it possible to see what happens on the surface when the components of the solution are adsorbed and when the electrode potential is altered. Investigators have become able not only to visualise the mechanism of the electrode process from coulometric, voltammetric, and optical data, as well as data obtained by structural methods, but have also acquired the capacity to 'see' how the atoms and molecules of the adsorbate are arranged, on which active centre the electrode reaction begins and proceeds at a high rate, what happens to the surface in adsorption–desorption processes, etc. So far, the STM is not able to provide answers to questions such as how the elementary step in the electrode process occurs, how the reaction is influenced by the scanning probe, and whether or not the processes occurring on the surface monitored by the probe and on other sections of the electrode are identical. However, there are no grounds for doubting that in the immediate future answers to these questions will be obtained with the aid of the combined use of STM, AFM, and optical and structural methods. However, even now, in the early stages of the development of scanning probe microscopy, many important results requiring comprehensive consideration have been obtained. We shall examine the latest results in this field.

1. Direct observation of the atomic structure of the electrode surface in solution

Even before the STM era, cyclic voltammetry and structural methods made it possible to establish that a change in the potential of the platinum electrode leads to the reconstruction of the surface layers, which is accelerated by oxygen adsorption-desorption processes. The reconstruction of the Pt(111) surface in sulfuric acid has been investigated by the STM method in situ.[57–60] It was established that when the potential is cycled in the range 0.10–0.65 V relative to the normal hydrogen electrode (NHE), the surface of platinum is stable as a function of time and extensive terraces with a monatomic height (0.23 nm) can be seen on it, while cyclic voltammetry (CVA) reveals a high degree of perfection of the Pt(111) single crystal [the shape of the curve resembles a butterfly, there are no distinct peaks corresponding to weakly and strongly bound hydrogen characteristic of a polycrystalline material, and at 0.45 V a sharp peak is observed and is caused, according to STM data obtained in situ, by an order–disorder transition in the monolayer of adsorbed bisulfate having a $(\sqrt{3} \times \sqrt{7})$ structure†].[60] If the potential is displaced to the hydrogen adsorption and evolution region, the CVA curve changes irreversibly and begins to resemble the curve characteristic of polycrystalline platinum,[57–60] while on the STM image a 'noise' appears. Further cycling in the range 0.05–1.5 V leads to an increase in the 'noise' on the image, although after five cycles the monatomic steps can still be seen and their distribution in space does not change.[60] The authors concluded that the adsorption–desorption of oxygen is accompanied by a rearrangement of the surface layers of platinum with the formation of randomly oriented islands 3–5 nm in diameter and with a height corresponding to 1–2 atoms: the adsorbed oxygen is incorporated in the surface layer and displaces some of the platinum atoms, which do not return to their former sites after the desorption of oxygen. It is not surprising that the rearranged surface gives rise to a CVA curve characteristic of a polycrystalline material.

The surfaces of platinum single crystals have been studied in detail[61] by the CVA and STM methods. It was established that the degree of ideality of the surfaces of the single crystals is greatly influenced by the preliminary treatment of the platinum before the electrochemical experiment and by the adsorption of oxygen during the recording of the CVA curve (thus the stage where the platinum heated in a hydrogen flame is cooled in water containing dissolved oxygen may 'spoil' the surface).

The Pt(111) surface, which is relatively insensitive (after heat treatment) to the presence of oxygen in the cooling water and is stable during cycling in the hydrogen and double layer regions, is rapidly spoiled when the potential shifts to +1.4 V (NHE): peaks due to weakly and strongly bound hydrogen appear on the CVA curve, the sharp peak at 0.45 V vanishes, and the STM images reveal a transformation of the atomically smooth terraces into grainy surfaces,[61] while low energy electron diffraction data indicate the loss of long-range order and the presence of a large number of randomly distributed surface defects,[62,63] which agrees well with the results of other studies.[57–60]

A surface of the Pt(100) single crystal has a lower reticular density and exhibits a greater tendency to undergo reconstructions.[64] A freshly polished Pt(100) face contains a large number of defects, which can be 'healed' by annealing at about 1000 °C with subsequent cooling in an oxygen-free atmosphere (cooling in iodine vapour, which is adsorbed on the platinum surface and prevents the influence of oxygen, yields the best results). According to STM and voltammetric data, the Pt(100) surface exhibits a high degree of ideality. The adsorption of oxygen on cooling or at high anodic potentials in solution leads to the appearance of a large number of linear surface defects along continuous rows of atoms: the STM image shows clearly a network of linear defects with rectangular cells, and in addition terraces are clearly seen.[61]

Rougher surfaces can also be observed with the aid of the STM. Polycrystalline platinum has been selected as the object of study.[65–68] After mechanical polishing, washing, and prolonged annealing, the platinum surface is entirely suitable for the investigation of oxidation processes, the electrodeposition of metals, the synthesis of conducting polymers, the mobility of atoms, etc. and even atomic resolution can be achieved on individual sections of the surface.

Gold single crystals have been studied in fair detail.[7,69–82] After treatment in a flame and cooling in pure water, the surface of Au(111) consisted of extensive atomically smooth terraces separated by monatomic steps.[7] The topography of the Au(100) surface was characterised by the presence of a large number of islands with a monatomic height. According to Nichols et al.,[69] the structural rearrangement of the denser hexagonal (5×20) lattice, formed on treatment of Au(100) in a flame, into the less dense cubic (1×1) surface, liberates approximately 20% of the surface atoms. These in fact form the above islands by surface diffusion.

The influence of the adsorption of anions and oxygen on the topography of Au(100) has been investigated.[69] The Au(100) surface is stable in 1 M H_2SO_4 solution at a potential of +0.4 V relative to the saturated calomel electrode, but the displacement of the potential into the +1.0 V region leads to the disappearance of the islands. A similar picture is observed in 50 mM H_2SO_4 + 5 mM HCl solution: the islands dissolve at +0.7 V. The polarisation of Au(100) at +1.25 V in 50 mM $HClO_4$ + 1 mM $Cu(ClO_4)_2$ solution leads to the appearance of a rough surface in which the height of the rugosities is ~1 nm as a result of the formation of oxides. But after the displacement of the potential into the double layer region, the surface is smoothed out — both the rugosities and the islands with a monatomic

† The $(\sqrt{3} \times \sqrt{7})$ structure corresponds to the sulfate superlattice in which the distances between the nodes are greater by factors of $\sqrt{3}$ and $\sqrt{7}$ than the distances between the atoms of the Pt(111) substrate.

height vanish. The authors explain this phenomenon by the increase in the mobility of the gold atoms following the adsorption of anions and the desorption of oxygen.

More vigorous oxidation of Au(111) (a film sputtered onto mica) in perchloric acid occurs when the electrode potential is cycled in the range 0.7–2.0 V relative to a quasi-equilibrium $Ag/AgClO_4$ electrode.[70,71] At potentials of 1.25 and 1.45 V, the CVA curve shows anodic peaks corresponding to the formation of gold oxide, whilst during the reverse scan the oxide is reduced at 1.05 V. At the anodic limit in the cycling of the potential of $E_a = 1.7$ V, small pits arise on the gold surface and rapidly disappear. At $E_a = 1.7$ V, the pits attain dimensions of the order of 4 nm and only vanish after 10 min. After intense oxidation ($E_a = 2.0$ V), many large pits are formed, the boundary of the terrace becomes curved, and the picture then remains unaltered until the introduction of 0.05 mM HCl into the solution. After this, the steps in the terrace become straightened in 15 min.[70] These findings confirm yet again that the fairly high mobility of the surface gold atoms increases still further in the presence of halides.[72] In contrast to gold, the defects on the surface of platinum, arising as a result of the adsorption–desorption of oxygen at high anodic potentials, are not healed during the experiment.[57–63]

The atomic structure of the unreconstructed Au(100) surface has been observed with the aid of the STM in situ.[73–74] The results of studies on the processes involved in the rearrangement of the Au(111), Au(110), and Au(100) surfaces as well as high-index gold faces by means of STM and AFM have been described.[75–82] Scanning probe microscopy has been used to investigate the state of the surfaces of silver,[83–87] copper,[88] carbon glass,[89] highly ordered pyrographite,[90,91] and other electrode materials, but their detailed consideration is outside the scope of the present review.

2. The study of adsorbed atomic layers

Adsorption with charge transfer, leading to the formation of adsorbed atomic layers at potentials more positive than the phase deposition potential [in the English language literature, the term underpotential deposition (UPD) has become established], has become the object of vigorous study during the last 20 years. There are several reasons for this. The structure and properties of adsorbed atomic layers differ from those of bulk-phase deposits; noble metals modified by adsorbed atoms possess unique catalytic properties (increased activity and selectivity, high resistance to catalyst poisons); the formation of adsorbed atomic layers is the first stage in the bulk-phase deposition of metals, the formation of nuclei on them being of fundamental interest in the study of the processes involved in nucleation and the growth of nuclei.

Voltammetry combined with coulometry and vacuum structural methods have been used traditionally to investigate the UPD. The development of SPM has led to new possibilities for monitoring in situ the state of the surface during the adsorption–desorption of atoms.

The deposition of copper on gold is one of the processes that has been investigated in greatest detail. A gold film 100 nm thick with the (111) texture, sputtered onto glass, was used as a support.[92] The reference electrode was a copper wire and the state of the surface was monitored with the aid of the AFM with atomic resolution.

The hexagonal structure of the Au(111) substrate with atomic distances of 0.29 nm is clearly observed at potentials more positive than the copper adsorption potential in sulfate (0.1 M H_2SO_4 + 1 mM $CuSO_4$) and perchlorate [0.1 M $HClO_4$ + 1 mM $Cu(ClO_4)_2$] solutions. Although the sulfate is adsorbed strongly at these potentials (+0.7 V relative to the copper reference electrode), its influence on the structure of the image was not observed. The authors explain this finding by the fact that the needle of the AFM displaces the adsorbed sulfate atoms during the scanning of the surface. A compressed hexagonal close-packed (HCP) Cu(111) copper layer with atomic distances of 0.26 nm (the atomic radii of Cu and Au are 0.175 and 0.142 nm respectively), rotated by 30° relative to the gold lattice, is observed at a cathodic overpotential of 0.05–0.10 V in both solutions after the deposition of several copper monolayers. Copper dissolves layer-by-layer and at +0.7 V the gold support without visible structural changes is observed, which indicates, according to the authors,[92] the complete reversibility of the adsorption–desorption process. This claim appears unduly dogmatic, since experiments in which AFM and STM are employed are carried out as a rule on the smoothest sections of the surface (otherwise atomic resolution cannot be achieved), while the reconstruction processes, induced for example by surface alloy formation, occur most vigorously on defects (dislocations, grain boundaries, etc.).[93]

An hexagonal close-packed copper monolayer with interatomic distances of 0.29 nm, rotated by 30° relative to the substrate, is observed in perchlorate solution at +0.11 V (the potential of the desorption peak on the CVA curve is +0.33 V), while the $(\sqrt{3} \times \sqrt{3})R30°$ open structure with interatomic distances of 0.49 nm is observed in sulfuric acid solution at +0.1 V. The same structure has been observed in situ with the aid of the STM in other investigations.[52,73,94,95] Similar results have been obtained in the analysis of the diffraction of low energy electrons.[96] Auger spectroscopy[97] of electrodes removed from the solution indicates the coadsorption of the sulfate. The adsorption of the sulfate on Au(111) in sulfuric acid solution has been investigated by IR spectroscopy and by means of STM in situ.[98] It has been shown that the SO_4^{2-} anion forms a $(\sqrt{3} \times \sqrt{7})$ superlattice with a degree of occupation of 0.2.

The $(\sqrt{3} \times \sqrt{3})R30°$ structure of the adsorbed copper atoms should correspond to a degree of filling of the monolayer of 1/3. In a sulfate electrolyte, there are two sharp desorption peaks on the CVA curve,[52,99] at +0.05 and +0.21 V, their areas being 0.15 and 0.30 mC cm^{-2} respectively, while the theoretical charge necessary for the adsorption of a monolayer (1×1) is 0.44 mC cm^{-2} (on the assumption of two-electron transfer), i.e. according to the coulometric data 2/3 of a monolayer is adsorbed at 0.1–0.15 V. Among the studies known to the authors, integration of the more anodic adsorption peak yielded a degree of occupation of 0.38 only in the study of Haiss et al.[95] This may be associated with the insufficiently low rate of scanning of the potential, since Shi and Lipkowski[99] maintained the electrode at the required potential for up to 10 min in order to obtain the equilibrium degree of adsorption. Furthermore, for determination of the degree of coverage it is better to employ the anodic branch of the CVA curve so as to eliminate the influence of the diffusion from the dilute solution on the adsorption kinetics.

Detailed thermodynamic analysis of the CVA curve showed[99,100] that the maximum coadsorption of the sulfate (one SO_4^{2-} ion on two adsorbed Cu atoms) occurs for degrees of coverage of the substrate by copper of $\theta = 0.25 - 0.7$ The $(\sqrt{3} \times \sqrt{3})R30°$ structure observed with the aid of STM and AFM corresponds to the adsorbed sulfate ions and not to copper atoms. Gordon et al.,[101] who investigated the adsorption of copper on gold by microgravimetry (quartz microbalance), EXAFS spectroscopy, the GIXS method (grazing incidence X-ray scattering or, more briefly, 'surface X-ray scattering'), which makes it possible to identify the surface structure from X-ray scattering data, and electrochemical methods, arrived at similar conclusions. The degree of charge transfer in the adsorption of copper is close to 2 and depends little on the potential. These results agree well with the multistage adsorption model,[102,103] according to which the adsorbed copper atoms substituted the SO_4^{2-} ions on the gold surface, arranged in such a way that the sulfur atom is located at the copper adsorption site, whilst three oxygen atoms are linked to three neighbouring gold atoms (Fig. 7).

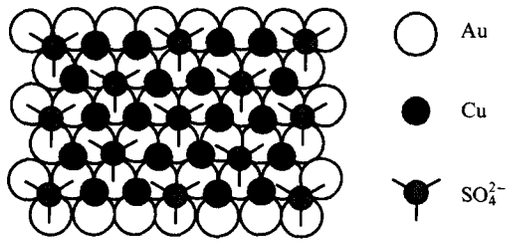


Figure 7. Schematic illustration of the structure of the adsorbate on Au(111) in sulfuric acid solution.

Several interesting features of the Au(111)/Cu/SO_4^{2-} system are noteworthy. Within the limits of a single atomically smooth Au(111) terrace, the sections of the $(\sqrt{3} \times \sqrt{3})R30°$ structure are separated by a phase boundary (the neighbouring rows of adsorbed sulfide ions are displaced to the 1/2 sites) — the situation is analogous to the formation of twinned crystals. At a potential of +0.2 V, the adsorbed copper atoms are partly desorbed [bands of the $(\sqrt{3} \times \sqrt{3})R30°$ lattice 5 – 10 nm wide and several nanometers long are observed].[52] The boundary of the $(\sqrt{3} \times \sqrt{3})R30°$ layer has been detected also in another study.[92] At +0.25 V, the lattice disappears completely, but the atomic resolution for the Au(111) surface cannot be achieved until the complete removal of the adsorbed atoms. At low coverages, the adsorbed copper atoms and sulfate ions apparently possess a high mobility (two-dimensional gas)[52,99] and their movement makes it impossible to obtain a clear-cut STM image.

When the electrolyte contains chloride ions (they can diffuse through the salt bridge when a calomel or a silver/silver chloride reference electrode is employed), the (5 × 5) lattice with interatomic distances of 0.37 nm is observed in addition to the $(\sqrt{3} \times \sqrt{3})R30°$ structure.[73] The STM yields an image comprising approximately ten $(\sqrt{3} \times \sqrt{3})R30°$ and (5 × 5) domains on a (22 × 22) nm section of the surface.[95] According to a study[104] of the coadsorption of copper atoms and halide ions on Au(111) and Pt(111) from 50 mM H_2SO_4 + 1 mM $CuSO_4$ + 0.1 mM KX (X = Cl^-, Br^-, I^-) solutions on gold at a potential of 285 mV (NHE), in the presence of chloride the STM records the (5 × 5) structure. In the bromide solution, the interatomic distances are increased by 6% [the (4 × 4) lattice relative to Au(111)], while in the presence of iodide a further increase in the adsorbate lattice parameter is noted — the (3 × 3) structure is observed [the same structure has been seen[105] on Au(111) in a study of the coadsorption of iodine and silver]. Coulometry yields a degree of coverage of the surface by adsorbed copper atoms (on the assumption of a two-electron transfer) equal to 0.4 of a monolayer regardless of the nature of the halide. According to the authors, the STM yields an image of the lattices of the chlorine, bromine, and iodine adsorbed on a layer of preadsorbed copper atoms, because an increase in the distances between the adsorbed atoms is correlated with the dimensions of the halides. It has been suggested that the adsorbed copper is partly discharged and stabilised by the anions.

Many fewer studies have been devoted to the UPD of copper on platinum.[104,106,107] This is apparently associated with the experimental difficulties in the preparation of platinum single crystals with a high degree of ideality and of clear-cut images of the surface with atomic resolution.

The first publication on the study of the UPD of copper on platinum with the aid of the STM in situ did not appear until 1991.[106] The substrate consisted of a Pt(111) single crystal treated in a burner flame; a 0.05 M H_2SO_4 + 5 mM $CuSO_4$ solution and a hydrogen reference electrode were used to prevent the contamination of the electrolyte with traces of chloride.

When the electrode potential is cycled in the range 0.5 – 0.8 V (NHE) at the rate 1 mV s^{-1}, a CVA curve with two sharp desorption peaks at potentials of 0.67 and 0.69 V and a half-width of about 5 mV is recorded. The overall charge in the desorption of adsorbed copper atoms is 460 μC cm^{-2} (this is twice as great as for the adsorbed hydrogen atoms in sulfuric acid); integration of the more anodic peak yields 270 μC cm^{-2}, which corresponds to approximately 60% coverage of the platinum surface by the adsorbed copper. A clear-cut image of the hexagonal $(\sqrt{3} \times \sqrt{3})R30°$ adsorbate structure with distances between the projections of about 0.5 nm was obtained at a potential of 0.68 V. The authors[106] believe that this is the lattice of adsorbed copper atoms and the discrepancy between the coulometric and STM data [we recall that a degree of monolayer coverage of 1/3, i.e. 160 μC cm^{-2}, and not the experimentally observed 270 μC cm^{-2} should correspond to the $(\sqrt{3} \times \sqrt{3})R30°$ superlattice] is explained by the effects due to the charging of the electrical double layer on desorption of the sulfate and bisulfate anions. However, such a large difference between the charges (110 μC cm^{-2}) can be hardly due to a non-Faraday process. Apparently, as in the case of the UPD of copper on Au(111),[52,73,92,95,100–103] the STM yields an image of the structure of the adsorbed sulfate.

At a potential of 0.8 V, the STM yields, with atomic resolution, the image of a nonperiodic structure in which the height of the projections is 0.04 – 0.06 nm and the average distance between them is 0.5 – 0.6 nm. It was not possible to obtain the image of the hexagonal Pt(111) lattice. On consecutive recording of several images of the same section of the surface, it was found that the disposition of the projections and hollows varies with time; this is probably associated with the mobility of the adsorbed sulfate and bisulfate ions.[106] The influence of organic additives on the UPD of copper on platinum has also been investigated in another study[107] with the aid of STM in situ, but it was not possible to record the structure of the adsorbate with a lateral (side) atomic resolution.

A study has been made[104] of the sorption of copper on platinum in the presence of halides from 50 mM H_2SO_4 + 1 mM $CuSO_4$ + 0.1 mM KX solutions, where $X^- = Br^-$ or I^-. An image of platinum with atomic resolution was obtained initially in sulfuric acid solutions at 380 mV (NHE) and the interatomic distances and the orientation of the substrate were determined. After this, in the solution with added KI the $(\sqrt{3} \times \sqrt{3})R30°$ structure was observed at the same potential for several hours. This superlattice was not observed in ex situ studies after the removal of the electrode from the cell; it apparently exists only in solution. The same structure has been observed in a solution with added KBr at a potential of 400 mV. In both cases, a copper monolayer (1 × 1) is deposited on the platinum surface according to coulometric data. The authors believe that the recorded $(\sqrt{3} \times \sqrt{3})R30°$ structure corresponds to a second layer of the superlattice consisting of iodide or bromide ions adsorbed on the copper monolayer [the $(\sqrt{3} \times \sqrt{3})R30°$ iodine lattice on Pt(111) in perchloric acid solution with added iodine has been observed by Yau et al.[108]].

The adsorption of lead atoms on silver single crystals may serve as an example of yet another system which has been studied in detail by means of electrochemical and structural methods and also in situ with the aid of STM.

Several absorption – desorption peaks in the UPD region have been observed on the CVA curve for the Ag(*hkl*)/Pb^{2+} system, which indicates the stepwise formation of dimeric monolayers with different superlattice structures depending on the crystallo-graphic orientation of the substrate and the electrode potential.[109] The use of the STM with lateral atomic resolution in situ demonstrated the formation on Ag(111) of a compressed HCP Pb monolayer, rotated by 4.5° relative to the lattice of the support, with distances between the nearest neighbours of 0.34 nm in the region of potentials more positive than the equilibrium value by 0 – 100 mV.[110]

A completely different picture is observed on Ag(100) in the same potential range. At 50 mV, the application of the STM in situ

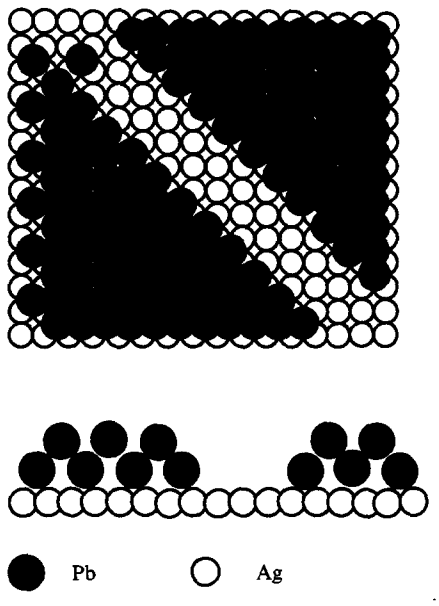


Figure 8. Schematic illustration of the two-layer $c(2 \times 2)$Pb–$c(2 \times 2)$Pb adsorption lattice with a twin boundary between the domains.

demonstrated the presence of a square lead superlattice with a relatively low reticular density. The symmetry of the superstructure and the distances between the first (0.40 nm) and second (0.59 nm) nearest neighbours are satisfactorily consistent with the 'Ag(100) upper layer–$c(2 \times 2)$–$c(2 \times 2)$Pb' double layer superlattice (Fig. 8), as postulated previously.[111] However, measurements of the degree of surface coverage, Monte Carlo mathematical modelling, and tunnelling microscope data indicate that the adsorbed lead atoms form ordered domains separated by boundaries (the chess board effect).[109]

At relatively high anodic potentials (more positive than the equilibrium value by 120–200 mV), the structure of the first Ag(100)–$c(2 \times 2)$Pb adsorbed layer cannot be observed with the aid of the STM. This can be explained by the high mobility of the adsorbed lead atoms at low and moderate surface coverages (the exchange current of the adsorbed lead atoms increases sharply at low surface coverages[112]). The Ag(100)–$c(2 \times 2)$Pb structure corresponds to $\theta = 0.5$ (each adsorbed atom occupies two adsorption sites in the square lattice), which also agrees well with the results of mathematical modelling for an energy of interaction between nearest neighbours of 2.5×10^{-21} J atom^{-1}.[113]

The structural transformation of the square Ag(100)–$c(2 \times 2)$–$c(2 \times 2)$Pb bilayer into a compressed HCP monolayer has been observed in situ with the aid of STM with the potential being varied from 50 mV to zero. It was postulated that this process begins at the boundaries of the ordered domains of the bilayer, the relative compression of the adsorption layer agreeing well with STM and X-ray scattering data for a hexagonal close-packed layer of adsorbed lead atoms on Ag(111).[109]

Thus, regardless of the crystallographic orientation of the silver substrate, the adsorbed lead atoms form an HCP Pb(111) monolayer. This unexpected result emphasises yet again the unique possibilities of the use of the STM in situ for the investigation of electrode processes.

In the Au(hkl)/Ag$^+$ system, there is a strong adsorbate–substrate interaction and the lattice parameters differ only slightly (0.2884 nm for gold and 0.2890 nm for silver), which makes it possible to expect the operation of the Frank–Van der Merwe mechanism, i.e. the formation of dimeric nuclei and subsequent layer-by-layer growth of the deposit. The silver adsorption–desorption process on gold depends greatly on the crystallographic orientation of the substrate. The degree of surface coverage by the adsorbed atoms was determined[109] from the anodic desorption curves after brief (not longer than 2 min) polarisation of the electrode in dilute (10^{-5}–10^{-3} M $AgClO_4$) solutions at the equilibrium silver deposition potential. The formation of noncompressed silver monolayers with an orientation epitaxial relative to the substrate was observed with the aid of the scanning tunnelling microscope.[109,114–119] In experiments with prolonged (of the order of 40 min) maintenance of the electrode at potentials close to the equilibrium value (0–15 mV), evidence for the formation of the Au–Ag alloy, beginning on the surface defects and the boundaries of the projections, was obtained.[119]

The UPD of silver on Au(111) in a sulfate solution has been investigated.[120] The $(\sqrt{3} \times \sqrt{3})R30°$ structure was observed for this system for the first time with the aid of the STM. According to coulometric data, this lattice corresponds to 1/3 of the silver monolayer. The authors attribute the STM image to the silver superlattice, but in this case the microscope can record both adsorbed silver atoms and sulfate anions (the probable structure of the adsorbate is illustrated schematically in Fig. 9). The results of a detailed study of this system with the aid of in situ and ex situ methods have been published.[121]

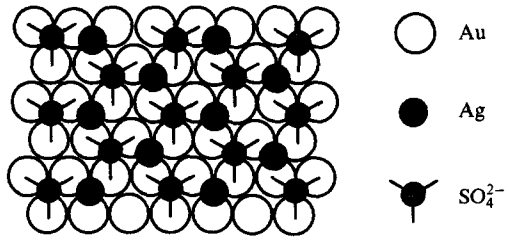


Figure 9. Schematic illustration of the $(Ag\sqrt{3} \times \sqrt{3})R30°$ adsorption lattice on Au(111).

The influence of the nature of the anion on the UPD of silver and mercury on Au(111) has been studied[117,122,123] with the aid of atomic force microscopy. It was shown that the mercury monolayers have an hexagonal structure with an interatomic distance of 0.58 nm (the crystal lattice parameter of solid mercury at low temperatures is 0.31 nm) in sulfate, nitrate, and perchlorate electrolytes. The adsorbed silver atoms are extremely sensitive to the size of the anion: the packing density of the adsorbate increases in the sequence sulfate (44%) < nitrate (56%) < perchlorate (64%) < acetate (100%, HCP).

The structure of the surface of gold modified by adsorbed atoms and its influence on the catalytic properties of gold have been investigated.[124–126] The structure of the bismuth monolayer on Au(111) depends on the applied potential: at potentials of 10–190 mV (more positive than the bulk-phase deposition potential), a rectangular $(p \times \sqrt{3})$ lattice, compressed along one of the axes and with an interatomic distance of 0.34 nm and a degree of surface coverage of about 60%, is formed. At potentials of 200–280 mV, there is a stable (2×2) phase with the angle $\theta = 0.25$ and a lattice parameter of 0.57 nm. The catalytic activity of the (2×2) structure in the oxidation of hydrogen peroxide is higher, since in this case the gold and bismuth atoms are accessible to the H_2O_2 molecules (Fig. 10). For the denser monolayer, only bismuth atoms are accessible, whilst for zero surface coverage only gold atoms are accessible. The maximum activity is observed when the Au and Bi atoms act jointly [124,125] When Au(111) is modified by adsorbed lead atoms, the potential at which the surface is coated by islands of the Pb(1×1) HCP phase corresponds to the highest catalytic activity,[126,127] whereas the clean surface of gold and the complete lead monolayer on Au(111) are catalytically inactive. The increased activity of the heterometallic centres is apparently associated with spatial effects

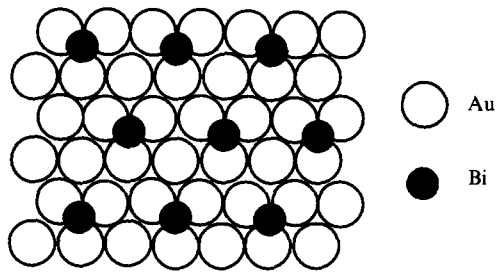


Figure 10. Schematic illustration of the Bi(2 × 2) adsorption lattice on Au(111).

and the different adsorption capacities of the adsorbed atoms and the surface atoms of the support in relation to oxygen and hydrogen atoms.

The examples of studies on the structures of adsorbed atomic layers examined here demonstrate convincingly that tunnelling and atomic force microscopes are powerful instruments for the study of adsorption processes. However, scanning probe microscopy cannot as yet do without the employment of traditional electrochemical methods (cyclic voltammetry, coulometry, etc.), in which the necessary requirements as regards purity in the experiments and in the preparation of the objects of study are met. Only comprehensive combined investigations make it possible to reach conclusions, with a high degree of reliability, about the mechanism of the adsorption process and the influence of various factors on the latter.

3. Scanning microscopy of the initial stages of the electrodeposition of metals

Scanning probe microscopy proved extremely useful for the investigation in situ of the initial stages of the electrocrystallisation and corrosion of metals, because the size of the nuclei of the new phase does not as a rule exceed several tens of atoms.[128,129] There are numerous publications devoted to the use of SPM for the observation of processes involving the phase deposition of metals from model and industrial electrolytes under potentiostatic, galvanostatic, and pulsed electrolytic conditions.[2,3,5,7,11,32–34,42,73,91,109,130–155] The influence of organic additives on the mechanism of electrocrystallisation has been studied in a series of investigations.[152–155] An increasing number of publications have been appearing on the use of SPM for the study of the structure and mechanism of formation of passive films in anodisation and also of the initial stages of corrosion processes.[156–166]

Despite the diversity of the systems investigated and the characteristic features of each of them, the following general conclusions can be made: (1) nucleus formation always begins on the active centres of the substrate, which consist of the projections on the boundaries of the terraces and of crystal lattice defects (as a rule, dislocations); (2) the nuclei of the new phase are formed later on the flat terraces, where the number of defects is small, and then on the defects themselves; (3) in the vast majority of studies, it has been concluded that the height of the nuclei is several times smaller than their transverse dimensions, which indicates a high energy of interaction of the atoms of the deposited metal with the atoms of the substrate.

We shall consider certain examples of the investigation of the initial stages of electrocrystallisation by use of the STM in situ. Generalised results of the study of the 'adsorption layer–phase' transition on the surface of gold in 10^{-5} M $AgClO_4$ solutions have been published.[109] The processes, involving the formation of a monolayer of adsorbed atoms and of the three-dimensional silver phase, are controlled by diffusion under these conditions and are slow. A special polarisation procedure, in which the electrode is maintained at specific potentials, was used to achieve the deposition of the required number of silver monolayers on gold. The number of monolayers was monitored coulometrically by the successive etching of the deposit. The formation of three-dimensional silver crystals was not observed microscopically up to the deposition of 40 monolayers. The mechanism of the layer-by-layer deposition of silver was supported by the formation of the lead UPD on such a silver deposit. Cyclic voltammetry in a lead-containing solution yields adsorption–desorption curves typical of the Ag(*hkl*)/Pb^{2+} systems, which are characteristic of the deposition of two or more silver monolayers on Au(*hkl*). Scanning tunnelling microscopy also indicates the layer-by-layer epitaxial growth of the silver deposit on Au(*hkl*). The uniform distribution of the deposit on the surface of the substrate is further confirmed by data obtained by scanning Auger spectrometry.[114–116]

In the deposition of fewer than two silver monolayers, slow alloy formation between the gold atoms of the surface layer and the silver atoms of the deposit is observed. In this case, CVA in solution with added lead gives rise to a curve with features characteristic of two systems: Ag(*hkl*)/Pb^{2+} and Au(*hkl*)/Pb^{2+}.

The observed layer-by-layer growth of the silver deposit on gold can occur in different ways depending on the degree of ideality of the substrate and on the overpotential.

1. The monolayer growth of a single nucleus on a surface free from screw dislocations at relatively low overpotentials (the growth of a new two-dimensional nucleus begins after the layer of silver has spread over the entire surface).

2. The formation of several nuclei on a surface free from screw dislocations at relatively high overpotentials and the subsequent growth of a packet of layers (polynuclear multilayer growth).

3. Multilayer spiral growth on the surface screw dislocations at low overpotentials.

In the study of the 'adsorption layer–phase' transition in more concentrated solutions (10^{-1} M $AgClO_4$), a time dependence of the current (current transients) with two characteristic sections was observed. For short times, the descending part of the transient corresponds to the formation of several monolayers of the deposit. The subsequent increase in the current is associated with the change in the nature of the deposition and the formation of three-dimensional multilayer growth packets. The dependence of the stationary current on the overpotential is evidence in support of the multilayer growth on the screw dislocations on the silver layers inherited from the gold substrate.[109]

The study of the phase deposition of lead on silver single crystals at potentials more negative than the equilibrium value showed that, regardless of the crystallographic orientation of the substrate, the lead films and three-dimensional crystallites have the (111) texture.[110,111,130–133] This means that the compressed two-dimensional HCP layer of adsorbed lead atoms constitutes the base for the subsequent epitaxial three-dimensional formation and growth of the bulk phase of lead. The influence of this sublayer on the nucleation process and the growth kinetics has been analysed on the basis of the atomistic theory of nucleation.[134]

Parallel monatomic steps have also been observed[135] in situ with the aid of STM in the three-dimensional growth of a lead film. According to the authors, these were generated by a screw dislocation (the image of an 80 × 80 nm section of the surface clearly shows five growth steps). The specific boundary energy of a monatomic step was estimated[135] from the average distance between the steps and the overpotential employed. It proved to be 3×10^{-14} J cm^{-1}.

Measurements of the tunnelling current under the conditions of a constant height of the probe above the electrode surface showed that the effective heights of the tunnelling barrier differ from the pure Ag(100) and Ag(111) substrates, whereas in the presence on the latter of a HCP monolayer of adsorbed lead atoms they are the same and are virtually equal to the height of the barrier for the Pb(111) bulk phase. For the Ag(100)–$c(2 \times 2)$–$c(2 \times 2)$Pb bilayer superlattice, which exists at potentials of

40 – 100 mV (more positive than the equilibrium value), the height of the tunnelling barrier is appreciably lower.[109]

These results demonstrate unambiguously that the Stranskii – Krastanov mechanism operates in the Ag(*hkl*)/Pb^{2+} system: a three-dimensional lead phase is formed on a silver substrate modified by a two-dimensional layer of adsorbed atoms.[110,130,131]

Electrolytes with organic additives are employed in the majority of technological processes to ensure the necessary decorative, protecting, and physicochemical properties of the galvanic coatings. The mechanism of the effect of the additives has always interested specialists and the introduction of SPM made it possible to obtain unique new information about this problem.

The influence of benzotriazole (BTA) on the nucleation and growth of copper crystals on platinum in sulfuric acid and perchlorate electrolytes has been investigated under potentiostatic and galvanostatic conditions.[152] The density of the nuclei was determined with the aid of a Fourier transformation of the profile of the surface of the deposit, and by assuming that the characteristic frequency of the rugosities of the profile is inversely proportional to the average width of the nucleus. It was shown that in the presence of BTA the faceting of the deposit is suppressed (the crystallites have a nearly hemispherical form) and the deposition overpotential increases appreciably, but the number of nuclei hardly changes.

Crystal Violet (CV) and benzotriazole derivatives were selected in other studies[153–155] as additives to sulfuric acid and perchlorate copper-plating electrolytes. The substrate was gold film sputtered onto glass and annealed in a burner flame in order to obtain the (111) texture. It was established that, in solutions without additives at overpotentials of 200 – 400 mV, instantaneous nucleation and three-dimensional growth of crystallites 1 – 10 nm high take place. The introduction of 10 mg $litre^{-1}$ of CV into the 0.1 M H_2SO_4 + 0.05 mM $CuSO_4$ solution suppresses the tangential growth of the crystals — their height does not exceed 1 nm. However, in a solution with 0.1 M H_2SO_4 + 1 mM $CuSO_4$ this additive hardly affects the morphology of the copper crystals.

Regardless of the presence of additives in the solution, the nucleation of the copper crystals takes place on defects; the nuclei are not formed on the flat defect-free terraces. The authors explain this finding by the greater size of the organic molecules, which cannot block tightly the steps and defects on the substrate, allowing access by the adsorbed copper atoms and ions to the nucleation and growth sites.

The influence of organic additives is manifested at later stages. In pure H_2SO_4 + $CuSO_4$ solution, copper crystallites have flat upper faces and stepped edges. In the presence of the benzotriazole derivative BT-A in 50 μM $CuSO_4$, a quasi-two-dimensional growth of the deposit takes place in the electrolyte, whilst in 1 mM $CuSO_4$ both planar and three-dimensional copper crystals are formed.

The addition of another benzotriazole derivative (BT-B) at a concentration of 10 mg $litre^{-1}$ has a more pronounced inhibiting effect. Regardless of the copper sulfate concentration, the tangential growth of the crystals is suppressed and their height does not exceed 1.5 nm.

An AFM with a wide-field (8 μm × 8 μm) piezoscanner was used to observe thicker deposits. In the deposition of copper from a 120 g $litre^{-1}$ $CuSO_4$ + 0.5 M H_2SO_4 solution at −74 mV, a thick deposit, in which the height of the rugosities is ~500 nm, is formed. In the presence of CV, the height of the crystallites reaches 10 nm [the thickness of the monatomic copper(111) layer is 0.209 nm], whilst in the presence of 10 mg $litre^{-1}$ of BT-B the lateral growth of layers with a thickness up to 1.5 nm (4 – 7 monolayers) takes place. These layers then grow together and the sites where this has taken place become the active centres for the nucleation of a new upper monolayer of copper. The authors attribute this sharp decrease in the thickness of the growing layer to the influence of the substrate. We may recall that the interatomic distances in the Cu(111) and Au(111) lattices are 0.256 and 0.289 nm respectively, while the UPD layer has a lattice parameter characteristic of the substrate. Furthermore the energy of the Cu – Au interaction is greater than that of the Cu – Cu interaction, which is indicated by the occurrence of the UPD and the formation of an alloy. The monolayer growth of copper on the extended UPD layer is apparently energetically unfavourable and the spreading of the packet of layers is accompanied by the relaxation of stresses.

The planar organic molecules of the additives are apparently more strongly adsorbed on the top of the growing layer than on the growth steps by virtue of steric factors. In this case, the inhibition of the vertical growth should be manifested to a greater extent than that of the lateral growth. The defects arising in the growing together of the lower layers may serve as the active centres for the nucleation of the new layer. Yet another factor promoting the lateral growth in the presence of additives is the overall inhibition of the process (the discharge of the ions and their incorporation into the lattice), which leads to the formation of less defective layers and hence to a decrease in the number of active centres for secondary nucleation. The principal conclusion reached by Nichols et al.[154] reduces to the statement that the form of the crystallites in electrodeposition is determined by the ratio of the rates of the secondary nucleation and the lateral growth, and that surface-active additives may alter this ratio.

An example of the use of SPM for the monitoring of the technological copper plating of printing plates is provided by another study of Nichols et al.[155] The atomic force microscope was used at the stage involving the preparation of the surface before chemical copper plating and the generation of the adhesion layer, and the STM was employed to investigate the initial stages of the electrocrystallisation of copper from industrial electrolytes with organic additives. Thus the STM has already ceased to be an instrument for purely theoretical research and is being used more frequently as an element of technological monitoring.

V. Prospects for the development of scanning probe microscopy

Naturally, the examples of the employment of SPM examined in the previous sections naturally did not exhaust all the possibilities of this method in relation to electrochemistry. Studies involving tunnelling and atomic force microscopy in biology and bioelectrochemistry,[5] organic electrochemistry, and the electrochemistry of semiconductors and conducting polymers have not been dealt with in this review, and certain studies on the corrosion of metals and alloys have only been touched upon — these require special consideration because the number of publications on these problems have been increasing every year and it is impossible to analyse them within the framework of a single article.

In concluding the survey of the latest advances in the use of SPM in the electrochemistry of surfaces and in the electrocrystallisation of metals, it is desirable to consider the problems and prospects for the development of this method. The inconsistency between the electrochemical parameters averaged over the entire electrode surface (the current – potential – time relations) and the local visual information about the structure of a small section of the electrode and the processes occurring on it (one cannot be certain that the processes under the probe and at a distance from it take place at the same rate) can apparently be regarded as the principal problem of the use of the STM in situ. The size of the tunnelling probe is so great compared with the distance between the latter and the test surface that diffusional and electrical shielding[93] or stimulation[145] [observed in the study of the deposition of copper on Cu(110) with the aid of the AFM] effects inevitably arise. In each specific case, investigators have endeavoured to take this influence into account by selecting

experimental conditions such that it can be neglected. However, they have not always been able to ensure an unambiguous interpretation of the results. The appearance in recent years of wide-field piezoscanners, capable of recording the image of a surface whose size runs into tens and even hundreds of micrometres, has made it possible to scan virtually the entire microelectrode surface with the exception of the edges (in this case, the working feedback loop would stick the probe into the dielectric material), but a satisfactory resolution is so far virtually unattainable over large areas.

The electrical conductivity of the object is not of fundamental importance for atomic force microscopy, so that the employment of the AFM for the analysis of the entire microelectrode surface might eliminate the problem of the correlation between electrochemical data and the topography (here it is necessary to take into account the possible activation of the surface by the probe[145]). The present authors are unaware of any publications of this kind, but the logic of the development of events suggests that they are to be expected in the immediate future.

Yet another problem is the recognition of the image. Scanning probe microscopy yields a picture of the surface, but it is by no means always clear what it represents. The studies on the copper UPD process on gold and platinum examined above may serve as an example. The question arises how one can distinguish an adsorbed copper atom from a sulfate ion. Tunnelling spectroscopy should apparently be relevant here, but the employment of STS in electrochemical systems has significant characteristic features. It has been shown[167] that the change in the electron work function on passing from one metal to another is compensated by the corresponding change in the Galvani potential, so that the rate of the electrode reaction (and also possibly the rate of the tunnelling of electrons to the probe) is independent of the electron work function and is determined solely by the electrode potential. In this case, the use of STS in solutions on metallic electrodes is impossible from the standpoint of the modern theory of the elementary step. However, measurements of the dependence of the tunnelling current on the height of the probe over the Ag(111) and Ag(100) substrates and the calculations of the effective tunnelling barriers have shown[109] that, for an identical potential of +300 mV relative to the Pb^{2+}/Pb electrode, these values are 0.35 ± 0.01 and 0.31 ± 0.01 eV respectively. In the presence of a lead monolayer on the surface of a silver single crystal, the height of the barrier is 0.17 ± 0.01 eV regardless of the potential (0 – 50 mV) and the crystallographic orientation of the substrate. Unfortunately, the potentials of the tunnelling probe in the measurement of the tunnelling barriers are not quoted in the communication of Staikov et al.[109] Such information might throw light on the situation. The resolution of this contradiction apparently requires careful theoretical and experimental studies on the application of STS in situ.

In discussing the prospects for the development of SPM, one can postulate that the range of objects and the different aspects of such investigations should greatly expand and that the method will be used with increasing frequency for the solution of technological problems. To a large extent, this concerns the problems of nanotechnology, which began to develop actively after the invention of the STM. The possibility of observing atomic structures led to the wish to modify the surface at the atomic level.[5,11] Investigators learnt how to draw letters and symbols with a line having a width of several nanometres, and studies on the construction of the nanoelements of integrated circuits, memory devices, elements for quantum electronics, etc. are being vigorously prosecuted. It appears that electrochemistry will not be neglected either. There have already been publications on the local (in the nanometre range) deposition and dissolution of metals, the study of electrode reactions on the surfaces of semiconductors[11] with the aid of the SPM, and the preparation of multilayer coatings with a monatomic thickness of the layers (sandwich heterostructures[109]). The development of tunnelling and atomic force microscopy has led to the development of a series of related methods,[4–6] and so called scanning electrochemical microscopy is extremely promising.[168–170] The essential feature of the method is that it employs as the probe a disc ultramicroelectrode 0.1 – 25 μm in diameter with insulated lateral surfaces on which a potential is maintained, thereby ensuring the occurrence of an electrochemical reaction — for example the oxidation of Cu^+ or the reduction of Cu^{2+} in the investigation of the dissolution of copper on the main electrode. The probe moves over the test surface and the distribution of the active dissolution centres can be inferred from the probe current.

The use of a probe as an auxiliary electrode permits selective deposition, the etching of metals and semiconductors in electrolytes with a low scattering capacity and in polymer films with ionic conductivity, and electropolymerisation. The resolution ensured by the method depends on the size of the probe, the distance between the microelectrode and the specimen, the electrolyte composition, and the electrolysis conditions and can reach 100 nm.[170] Satisfactory results have been obtained when probes consisting of very sharp noninsulated needles were employed.

A probe can be used as a reference electrode and the distribution of the surface potential can be monitored, for example, in the study of corrosion processes.[171,172] The method is called scanning potentiometry and has a very low resolution.

Yet another promising aspect of the development of SPM involves the creation of combined instruments, in which tunnelling and atomic force microscopy as well as its variations are combined with other in situ methods (optical, acoustic, microgravimetric, etc.). Such studies are already being carried out[13–17] and the first results give rise to the hope for their successful development.

Binnig and Rohrer, the inventors of the STM, entitled their Nobel lecture in 1986 'Scanning Tunnelling Microscopy — From Birth to Youth'. Likewise one may say that the youth of scanning tunnelling microscopy has now ended and that it is now an entirely serious method which has justified the boldest hopes concerning it. Scanning probe microscopy is entering the period of maturity and is used very productively in most diverse fields of science and technology. However, its main attainments still remain in the future.

The review has been written with the financial support of the Russian Fundamental Research Fund (projects 93-03-4002 and 95-03-08100), the International Scientific Fund, and the Government of Russia (projects M4X000 and M4X300).

References

1. G Binnig, G Rorer *Usp. Fiz. Nauk* **154** 261 (1988)
2. R J Behm, N Garcia, H Rohrer (Eds) *Scanning Tunneling Microscopy and Related Methods* (NATO ASI Series, Ser. E: Applied Sciences, Vol. 184) (Erice, Italy: Kluwer, 1989)
3. T R I Cataldi, I G Blackham, G A D Briggs, J B Pethica, H A O Hill *J. Electroanal. Chem.* **290** 1 (1990)
4. H-J Guntherodt, R Wiesendanger (Eds) *Scanning Tunneling Microscopy, I. General Principles and Applications to Clean and Adsorbate-Covered Surfaces* (Springer Series in Surface Sciences, Vol. 20) (Berlin: Springer, 1992)
5. R Wiesendanger, H-J Guntherodt (Eds) *Scanning Tunneling Microscopy, II. Further Applications and Related Scanning Techniques* (Springer Series in Surface Sciences, Vol. 28) (Berlin: Springer, 1992)
6. R Wiesendanger, H-J Guntherodt (Eds) *Scanning Tunneling Microscopy, III. Theory of STM and Related Scanning Probe Methods* (Springer Series in Surface Sciences, Vol. 29) (Berlin: Springer, 1993)
7. D M Kolb, R J Nichols, R J Behm, in *Electrified Interfaces in Physics, Chemistry and Biology* (Ed. R Guidelli) (Netherlands: Kluwer, 1992) p. 275
8. P A Christensen *Chem. Soc. Rev.* **21** 197 (1992)
9. M Weaver, X Gao *Annu. Rev. Phys. Chem.* **44** 459 (1993)
10. X Gao, M Weaver *Ber. Bunsenges. Phys. Chem.* **97** 507 (1993)

11. A M Dykhne, O A Petrii, G A Tsirlina *Ross. Khim. Zh.* (*Zh. Ross. Khim. O-va im. D I Mendeleeva*) **38** 24 (1994)
12. G Binnig, C F Quate, Ch Gerber *Phys. Rev. Lett.* **56** 930 (1986)
13. L A Wenzler, T Han, R S Bryner, T R Beebe *Rev. Sci. Instrum.* **65** 85 (1994)
14. L M Eng, K D Jandt, D Descouts *Rev. Sci. Instrum.* **65** 390 (1994)
15. A V Ermakov, E L Garfunkel *Rev. Sci. Instrum.* **65** 2853 (1994)
16. T Goddenhenrich, S Muller, C Heiden *Rev. Sci. Instrum.* **65** 2870 (1994)
17. S Fujisawa, M Ohta, T Konishi, Y Sugawara, S Morita *Rev. Sci. Instrum.* **65** 644 (1994)
18. R M Feenstra, J A Stroscio, J Tersoff, A P Fein *Phys. Rev. Lett.* **58** 1192 (1987)
19. R S Becker, J A Golovchenko, D R Hamann, B S Swartzentruber *Phys. Rev. Lett.* **55** 2032 (1985)
20. R J Hamers, R M Tromp, J E Demuth *Phys. Rev. Lett.* **56** 1972 (1986)
21. E Tomita, N Matsuda, K Itaya *J. Vac. Sci. Technol. A, Vac. Surf. Films* **8** 534 (1990)
22. G Binnig, D P E Smith *Rev. Sci. Instrum.* **57** 1688 (1986)
23. L A Nagahara, T Thundat, S M Lindsay *Rev. Sci. Instrum.* **60** 3128 (1989)
24. H Liu, F-R F Fan, C W Lin, A J Bard *J. Am. Chem. Soc.* **108** 3838 (1986)
25. P J Bryant, H S Kim, Y C Zheng, R Yang *Rev. Sci. Instrum.* **58** 1115 (1987)
26. L Libioulle, Y Houbion, J-M Gilles *Rev. Sci. Instrum.* **66** 97 (1995)
27. A J Melmed *J. Vac. Sci. Technol. B, Microelectron. Nanometer Struct.* **9** 601 (1991)
28. B W Mao, J H Ye, X D Zhuo, J Q Mu, Z D Fen, Z W Tian *Ultramicroscopy* **42–44** 464 (1992)
29. C E Bach, R J Nichols, W Beckmann, H Meyer, A Schulte, J O Besenhard, P D Jannakoudakis *J. Electrochem. Soc.* **140** 1281 (1993)
30. C E Bach, R J Nichols, H Meyer, J O Besenhard *Surf. Coat. Technol.* **67** 139 (1994)
31. A A Gewirth, D H Craston, A J Bard *J. Electroanal. Chem.* **261** 477 (1989)
32. D J Trevor, C E D Chidsey, D N Loiacono *Appl. Phys. Lett.* **62** 929 (1989)
33. J Weichers, T Twomey, D M Kolb, R J Behm *J. Electroanal. Chem.* **248** 451 (1988)
34. M P Green, K J Hanson, D A Scherson, X Xing, M Richter, P N Ross, R Carr, I Lindau *J. Phys. Chem.* **93** 2181 (1989)
35. A J Bard, L Faulkner *Electrochemical Methods. Fundamentals and Applications* (New York: Wiley, 1980)
36. K Itaya, E Tomita *Surf. Sci.* **201** L507 (1988)
37. K Uosaki, H Kita *J. Electroanal. Chem.* **259** 301 (1989)
38. K Uosaki, H Kita *J. Vac. Sci. Technol. A, Vac. Surf. Films* **8** 520 (1990)
39. F-R F Fan, A J Bard *J. Electrochem. Soc.* **136** 3216 (1989)
40. R Christoph *Electrochim. Acta* **34** 1101 (1989)
41. R S Robinson *J. Microsc.* **152** 541 (1988)
42. Z W Tian, X D Zhuo, J Q Mu, J H Ye, Z D Fen, B W Mao, C L Bai, C D Dai *Ultramicroscopy* **42–44** 460 (1992)
43. J W G Wildoer, A J A van Roy, H van Kempen, C J P M Harmans *Rev. Sci. Instrum.* **65** 2849 (1994)
44. D N Davydov, R Deltour, N Horii, V A Timofeev, A S Grokholski *Rev. Sci. Instrum.* **64** 3153 (1993)
45. I B Altfeder, A P Volodin *Rev. Sci. Instrum.* **64** 3157 (1993)
46. X Liu, S T Smith, D G Chetwynd *Rev. Sci. Instrum.* **64** 3161 (1993)
47. A Cricenti, R Generosi, S Selci *Rev. Sci. Instrum.* **65** 80 (1994)
48. J W G Wildoer, A J A van Roy, H van Kempen, C J P M Harmans *Rev. Sci. Instrum.* **65** 2849 (1994)
49. M M Dovek, M J Heben, C A Lang, N S Lewis, C F Quate *Rev. Sci. Instrum.* **59** 2333 (1988)
50. J Wiechers, T Twomey, D M Kolb, R J Behm *J. Electroanal. Chem.* **248** 451 (1988)
51. J H White, H D Abruna *J. Phys. Chem.* **94** 894 (1990)
52. T Hachiya, H Honbo, K Itaya *J. Electroanal. Chem.* **315** 275 (1991)
53. S Park, C F Quate *J. Appl. Phys.* **62** 312 (1987)
54. J E T Andersen, P Moller *Surf. Coat. Technol.* **67** 213 (1994)
55. V Yu Yurov, A N Klimov *Rev. Sci. Instrum.* **65** 1551 (1994)
56. E P Stoll *Rev. Sci. Instrum.* **65** 2864 (1994)
57. S Sugawara, K Itaya *J. Chem. Soc. Faraday Trans. 1* **85** 1351 (1989)
58. K Itaya, S Sugawara, K Sashikata, N Furuya *J. Vac. Sci. Technol. A, Vac. Surf. Films* **8** 515 (1990)
59. K Sashikata, N Furuya, K Itaya, *J. Vac. Sci. Technol. B, Microelectron. Nanometer Struct.* **9** 457 (1991)
60. A M Funtikov, U Linke, U Stimming, R Vogel *Surf. Sci. Lett.* (1995) (in the press)
61. J M Feliu, F Rodes, J M Orts, J Clavilier *Pol. J. Chem.* **68** 1575 (1994)
62. F T Wagner, P N Ross *Surf. Sci.* **160** 302 (1985)
63. D Aberdam, R Durand, R Faure, F El Omar *Surf. Sci.* **171** 303 (1986)
64. I Villegas, M J Weaver *J. Electroanal. Chem.* **373** 245 (1994)
65. Y-M Wuu, F-R F Fan, A J Bard *J. Electrochem. Soc.* **136** 885 (1989)
66. K Itaya, K Higaki, S Sugawara *Chem. Lett.* 421 (1988)
67. C Alonso, R C Salvarezza, J M Vara, A J Arvia, L Vazquez, A Bartolome, A M Baro *J. Electrochem. Soc.* **137** 2161 (1990)
68. M Szklarczyk, J O'M Bockris *Surf. Sci.* **241** 54 (1991)
69. R J Nichols, O M Magnussen, J Hotlos, T Twomey, R J Behm, D M Kolb *J. Electroanal. Chem.* **290** 21 (1990)
70. D J Trevor, C E D Chidsey, D N Loiacono *Phys. Rev. Lett.* **62** 929 (1989)
71. X-P Gao, M J Weaver *J. Electroanal. Chem.* **367** 259 (1994)
72. X-P Gao, M J Weaver *J. Am. Chem. Soc.* **114** 8544 (1992)
73. O M Magnussen, J Hotlos, R J Nichols, D M Kolb, R J Behm *Phys. Rev. Lett.* **64** 2929 (1990)
74. N Batina, A S Dakkouri, D M Kolb *J. Electroanal. Chem.* **370** 87 (1994)
75. S Manne, J Massie, V B Elings, P K Hansma, A A Gewirth *J. Vac. Sci. Technol. B, Microelectron. Nanometer Struct.* **9** 950 (1991)
76. N J Tao, S M Lindsay *Surf. Sci.* **274** L546 (1992)
77. N J Tao, S M Lindsay *J. Appl. Phys.* **70** 5141 (1991)
78. X Gao, A Hamelin, M J Weaver *Phys. Rev. B* **44** 10983 (1991)
79. X Gao, A Hamelin, M J Weaver *Phys. Rev. Lett.* **67** 618 (1991)
80. X Gao, A Hamelin, M J Weaver *Phys. Rev. B* **46** 7096 (1992)
81. X Gao, A Hamelin, M J Weaver *Surf. Sci.* **274** L588 (1992)
82. G J Edens, X P Gao, M J Weaver *J. Electroanal. Chem.* **376** 21 (1994)
83. M L Foresti, A M Funtikov, R Guidelli, M Muniz-Miranda *J. Electroanal. Chem.* **367** 223 (1994)
84. G Aloisi, M Muniz-Miranda, R Guidelli, A M Funtikov, V E Kazarinov *Mendeleev Commun.* 244 (1993)
85. G Aloisi, A M Funtikov, R Guidelli *Surf. Sci.* **296** 291 (1993)
86. G Aloisi, A M Funtikov, T Will *J. Electroanal. Chem.* **370** 297 (1994)
87. B Wichman, J P van der Eerden, H Meekes, J Gerritsen *Electrochim. Acta* **37** 2331 (1992)
88. B J Cruickshank, D D Sneddon, A A Gewirth *Surf. Sci.* **281** L308 (1993)
89. P Heiduschka, A W Munz, W Gopel *Electrochim. Acta* **39** 2207 (1994)
90. B Keita, L Nadjo *J. Electroanal. Chem.* **354** 295 (1993)
91. A A Gewirth, A J Bard *J. Phys. Chem.* **92** 5563 (1988)
92. S Manne, P K Hansma, J Massie, V B Elings, A A Gewirth *Science* **251** 183 (1991)
93. R J Nichols, D M Kolb, R J Behm *J. Electroanal. Chem.* **313** 109 (1991)
94. O M Magnussen, J Hotlos, G Beitel, D M Kolb, R J Behm *J. Vac. Sci. Technol. B, Microelectron. Nanometer Struct.* **9** 969 (1991)
95. W Haiss, D Lackey, J K Sass, H Meier, R J Nichols *Chem. Phys. Lett.* **200** 343 (1992)
96. Y Nakai, M S Zei, D M Kolb, G Lehmpfuhl *Ber. Bunsenges. Phys. Chem.* **88** 340 (1984)
97. M S Zei, G Qiao, G Lehmpfuhl, D M Kolb *Ber. Bunsenges. Phys. Chem.* **91** 349 (1987)
98. G J Edens, X P Gao, M J Weaver *J. Electroanal. Chem.* **375** 357 (1994)
99. Z Shi, J Lipkowski *J. Electroanal. Chem.* **365** 303 (1994)
100. Z Shi, S Wu, J Lipkowski *Electrochim. Acta* **40** 9 (1995)
101. J G Gordon, O R Melroy, M F Toney *Electrochim. Acta* **40** 3 (1995)

102. D A Huckaby, L Blum *J. Electroanal. Chem.* **315** 255 (1991)
103. L Blum, D A Huckaby *J. Electroanal. Chem.* **375** 69 (1994)
104. H Matsumoto, I Oda, J Inukai, M Ito *J. Electroanal. Chem.* **356** 275 (1993)
105. S Sugita, T Abe, K Itaya *J. Phys. Chem.* **97** 8780 (1993)
106. K Sashikata, N Furuya, K Itaya *J. Electroanal. Chem.* **316** 361 (1991)
107. M Wunsche, R J Nichols, R Schumacher, W Beckmann, H Meyer *Electrochim. Acta* **38** 647 (1993)
108. S-L Yau, C M Vitus, B C Schardt *J. Am. Chem. Soc.* **112** 3677 (1990)
109. G Staikov, K Juttner, W J Lorenz, E Budevski *Electrochim. Acta* **39** 1019 (1994)
110. W Obretenov, U Schmidt, W J Lorenz, G Staikov, E Budevski, D Carnal, U Muller, H Siegenthaler, E Schmidt *J. Electrochem. Soc.* **140** 692 (1993)
111. W J Lorenz, E Schmidt, G Staikov, H Bort *Faraday Symp. Chem. Soc.* **12** 14 (1977)
112. M Klimmeck, K Juttner *Electrochim. Acta* **27** 83 (1982)
113. J P Van der Erden, G Staikov, D Kaschiev, W J Lorenz, E Budevski, M Hopfner, W Obretenov, K Juttner *Surf. Sci.* **82** 364 (1979)
114. H J Pauling, K Juttner *Electrochim. Acta* **37** 2237 (1992)
115. K Juttner, H J Pauling *Bull. Electrochem.* **8** 218 (1993)
116. H J Pauling, Ibrahim H Omar, K Juttner *Metalloberfläche* **47**(2) 66 (1993)
117. C-h Chen, A A Gewirth *Ultramicroscopy* **42–44** 437 (1992)
118. S G Corcoran, G S Chakarova, K Siradzki *Phys. Rev. Lett.* **71** 1585 (1993)
119. S G Corcoran, G S Chakarova, K Siradzki *J. Electroanal. Chem.* **377** 85 (1994)
120. T Hachiya, K Itaya *Ultramicroscopy* **42–44** 445 (1992)
121. P Mrozek, Y-E Sung, M Han, M Gamboa-Aldeco, A Wieckowski, C-h Chen, A A Gewirth *Electrochim. Acta* **40** 17 (1995)
122. C-h Chen, S M Vesecky, A A Gewirth *J. Am. Chem. Soc.* **114** 451 (1992)
123. C-h Chen, A A Gewirth *Phys. Rev. Lett.* **68** 1571 (1992)
124. C-h Chen, K D Kepler, A A Gewirth, B M Ocko, J Wang *J. Phys. Chem.* **97** 7290 (1993)
125. C-h Chen, A A Gewirth *J. Am. Chem. Soc.* **114** 5439 (1992)
126. C-h Chen, N Washburn, A A Gewirth *J. Phys. Chem.* **97** 9754 (1993)
127. M P Green, K J Hanson, R Carr, I Lindau *J. Electrochem. Soc.* **137** 3493 (1990)
128. A I Danilov, Yu M Polukarov *Usp. Khim.* **56** 1082 (1987) [*Russ. Chem. Rev.* **56** 619 (1987)]
129. A I Danilov *Ross. Khim. Zh. (Zh. Ross. Khim. O-va im. D. I. Mendeleeva)* **37** 63 (1993)
130. G Staikov, E Budevski, M Hopfner, W Obretenov, W J Lorenz, K Juttner *Surf. Sci.* **248** 234 (1992)
131. W J Lorenz, L M Gassa, U Schmidt, W Obretenov, G Staikov, V Bostanov, E Budevski *Electrochim. Acta* **37** 2173 (1992)
132. W Obretenov, U Schmidt, W J Lorenz, G Staikov, E Budevski, D Carnal, U Muller, H Siegenthaler, E Schmidt *Faraday Discuss. R. Soc. Chem.* **94** 107 (1992)
133. G Staikov, E Budevski, W Obretenov, W J Lorenz *J. Electroanal. Chem.* **349** 335 (1993)
134. A Milchev, S Stoyanov, R Kaishev *Thin Solids Films* **22** 267 (1974)
135. G Staikov, W Obretenov, V Bostanov, E Budevski, H Bort *Electrochim. Acta* **25** 1619 (1980)
136. J E T Andersen, G Bech-Nielsen, P Moller *Surf. Coat. Technol.* **67** 151 (1994)
137. J E T Andersen, G Bech-Nielsen, P Moller *Surf. Coat. Technol.* **70** 87 (1994)
138. W Li, J A Virtanen, R M Penner *Appl. Phys. Lett.* **60** 1181 (1992)
139. P Herrasti, P Ocon, R C Salvarezza, J M Vara, L Vazquez, A J Arvia *Electrochim. Acta* **37** 2209 (1992)
140. M E Martins, R C Salvarezza, A J Arvia *Electrochim. Acta* **37** 2203 (1992)
141. W U Schmidt, R C Alkire *J. Electrochem. Soc.* **141** L85 (1994)
142. D R Yaniv, L D McCormick *Electroanalysis* **3** 103 (1991)
143. Z F Chen, J Li, E K Wang *J. Electroanal. Chem.* **373** 83 (1994)
144. R Sonnenfeld, B C Schardt *Appl. Phys. Lett.* **49** 1172 (1986)
145. J R LaGraff, A A Gewirth *J. Phys. Chem.* **98** 11246 (1994)
146. M Szklarczyk, J O'M Bockris *J. Electrochem. Soc.* **137** 452 (1990)
147. K Itaya, S Sugawara *Chem. Lett.* **10** 1927 (1987)
148. K Itaya, S Sugawara, Higaki *J. Phys. Chem.* **92** 6714 (1988)
149. M J Armstrong, R H Muller *J. Electrochem. Soc.* **136** 584 (1989)
150. L Vazquez, A Hernandez Creus, P Carro, P Ocon, P Herrasti, C Palacio, J M Vara, R C Salvarezza, A J Arvia *J. Phys. Chem.* **96** 10454 (1992)
151. S A Hendrics, Y-T Kim, A J Bard *J. Electrochem. Soc.* **139** 2818 (1992)
152. M J Armstrong, R H Muller *J. Electrochem. Soc.* **138** 2303 (1991)
153. R J Nichols, W Beckmann, H Meyer, N Batina, D M Kolb *J. Electroanal. Chem.* **330** 381 (1992)
154. R J Nichols, C E Bach, H Meyer *Ber. Bunsenges. Phys. Chem.* **97** 1012 (1993)
155. R J Nichols, D Schroer, H Meyer *Scanning* **15** 266 (1993)
156. R M Rynders, C-H Paik, R Ke, R Alkire *J. Electrochem. Soc.* **141** 1439 (1994)
157. V Maurice, W P Yang, P Marcus *J. Electrochem. Soc.* **141** 3016 (1994)
158. V Maurice, H Talah, P Marcus *Surf. Sci. Lett* **284** L431 (1993)
159. V Maurice, H Talah, P Marcus *Surf. Sci.* **304** 98 (1994)
160. O Lev, F-R F Fan, A J Bard *J. Electrochem. Soc.* **135** 783 (1994)
161. F-R F Fan, A J Bard *J. Electrochem. Soc.* **136** 166 (1994)
162. R C Bhardwaj, A Gonzalez-Martin, J O'M Bockris *J. Electrochem. Soc.* **138** 1901 (1991)
163. Y C Wu, H W Pickering, D S Gregory, S Geh, T Sakurai *Surf. Sci.* **246** 468 (1991)
164. J Y Josefowicz, L Xie, G C Farrington *J. Phys. Chem.* **97** 11995 (1993)
165. N Nagashima, H Masuda, S Matsuoka *JSME Int. J. I* **35** 442 (1992)
166. G M Brown, T Thundat, D P Allison, R J Warmack *J. Vac. Sci. Technol. A, Vac. Surf. Films* **10** 3001 (1992)
167. B B Damaskin, O A Petrii, in *Vvedenie v Elektrokhimicheskuyu Kinetiku* (Introduction to Electrochemical Kinetics) (Moscow: Vysshaya Shkola, 1975) p. 247
168. A J Bard, F-R F Fan, J Kwak, O Lev *Anal. Chem.* **61** 132 (1989)
169. A J Bard, F-R F Fan, D T Pierce, P R Unwin, D O Wiff, F Zhou *Science* **254** 68 (1991)
170. A J Bard, G Denuault, C Lee, D Mandler, D O Wiff *Acc. Chem. Res.* 1990 **23** 357 (1990)
171. I L Rosenfeld, I S Danilov *Corros. Sci.* **7** 129 (1967)
172. H S Isaacs, M W Kendig *Corrosion* **36** 269 (1980)